Check for updates

THE AMERICAN SOCIETY OF MECHANICAL ENGINEERS
345 E. 47th St., New York, N.Y. 10017

96-GT-545

The Society shall not be responsible for statements or opinions advanced in papers or discussion at meetings of the Society or of its Divisions or Sections, or printed in its publications. Discussion is printed only if the paper is published in an ASME Journal. Authorization to photocopy material for internal or personal use under circumstance not falling within the fair use provisions of the Copyright Act is granted by ASME to libraries and other users registered with the Copyright Clearance Center (CCC) Transactional Reporting Service provided that the base fee of $0.30 per page is paid directly to the CCC, 27 Congress Street, Salem MA 01970. Requests for special permission or bulk reproduction should be addressed to the ASME Technical Publishing Department.

Copyright © 1996 by ASME All Rights Reserved Printed in U.S.A

REDUCTION OF NO_x FORMATION BY WATER SPRAYS IN STRAINED TWO-STAGE FLAMES

S.C. Li, N. Ilincic and F.A. Williams
Center for Energy and Combustion Research
Department of Applied Mechanics and Engineering Sciences
University of California, San Diego
La Jolla, CA 92093-0411

ABSTRACT

Staged combustion can be employed to reduce the formation of CO and NO_x, stabilize the flame, decrease the flame temperature and create better working conditions in gas turbine combustors. To help understand influences of partial premixing and addition of water on NO_x formation, we study two-stage flames in a counterflow spray burner. This paper reports experimental and theoretical results concerning two-stage combustion in which one feed stream is composed of a fuel-rich mixture of methane and air and the other is air. Water sprays are added to the air stream. This two-phase laminar counterflow configuration exhibits a green premixed flame, a blue diffusion flame and a vaporization plane. All three are flat and parallel. The separation distances between them decrease with increasing equivalence ratio and strain rate. Flow visualization is provided through illumination by an argon ion laser sheet, velocity fields and spray structure are measured by a phase-doppler particle analyzer, concentration fields of major stable species are measured by gas chromatography of samples withdrawn from the flame, and temperature fields are measured by a thermocouple. Numerical integrations which employ a recent chemical-kinetic data base are performed to model the flame structure and NO_x formation. Comparisons of experimental results with numerical predictions are made to test agreement. This work provides information on hydrocarbon combustion in both premixed flames and diffusion flames, indicates how NO_x is formed in fuel-rich flames and suggests how the pollutants can be reduced.

NOMENCLATURE

a	strain rate (s^{-1})
D_{23}	Sauter mean diameter
L	distance between the jet exits
L_s	separation distance between the air duct exit and the stagnation plane
M_i	molecular weight of i-th species
Q_F	volumetric flow rate of methane in fuel-air stream
Q_+	total volumetric flow rate of fuel-air stream
Q_-	total volumetric flow rate of air stream
r	radial coordinate
T	gas temperature
t	time
u	radial gas velocity
w	axial gas velocity
w_p	axial droplet velocity
X_i	mole fraction of i-th species
Y_i	mass fraction of i-th species
Y_W	mass fraction of water added in the air stream

Presented at the International Gas Turbine and Aeroengine Congress & Exhibition
Birmingham, UK — June 10-13, 1996
This paper has been accepted for publication in the Transactions of the ASME
Discussion of it will be accepted at ASME Headquarters until September 30, 1996

Downloaded from http://asmedigitalcollection.asme.org/GT/proceedings-pdf/GT1996/78743/V003T06A053/2407413/v003t06a053-96-gt-545.pdf by guest

z	axial coordinate
Φ	equivalence ratio of the fuel-air mixture
ρ	gas density
$\dot{\omega}_i$	molar production rate of species i

INTRODUCTION

Staged combustion is employed in many practical applications. In some cases, staged burners are designed to reduce the emissions of CO and NO_x [1]. There are many attractive concepts for reduction of NO_x emissions from gas turbines [2]. In one promising design for aircraft gas turbines, the combustor employs a two-stage combustion mechanism [3]; there is a fuel-rich combustion stage with equivalence ratio between 1.2 and 1.8, in which abundant hydrocarbon fuel rapidly consumes oxygen, and a fuel-lean combustion stage with equivalence ratio around 0.5, in which partially burned fuel from the previous stage burns practically completely after it mixes with newly introduced hot air. The formation of pollutants can be minimized in this design, and the turbine combustor can work under less harsh conditions, since the flame temperatures are relatively low.

In order to understand combustion processes in such flames and to identify the dominant reactions that lead to NO_x formation, experiments and numerical computations are performed here for a two-stage methane flame. To provide simple boundary conditions for the numerical modeling and to study the influences of sprays on the two-stage combustion, the present study employs an axisymmetric counterflow burner in which a rich fuel-air stream from one circular duct flow against an air stream from another circular duct. The boundary conditions at the exit of each duct are well defined, and therefore comparisons between experiment and theory can be made more easily. The influences of sprays on the formation of NO_x can be studied by adding sprays to either one of the two streams without difficulty. Further advantages of the the present configuration are that it affords ready access for instrumentation, that the experiments are relatively easy to perform, and that comparisons between theory and experiment are facilitated because the conservation equations are reduced to ordinary differential equations whose numerical analysis is thereby simplified.

A few of experimental and computational studies of partially premixed diffusion flames for purely gaseous fuels have been performed for counterflowing streams, one fuel rich and the other fuel lean [4-6]. Because the equivalence ratio was larger than 10 in the fuel-rich stream and smaller than 0.5 in the fuel-lean stream, all reactions occured in a relatively narrow zone, so that the flame was essentially a diffusion flame. In contrast to those studies, the present study is focused on two-stage combustion in which a fuel-rich stream with equivalence ratio between 1.3 and 3.0 is directed against a spray-air stream.

In a series of experimental studies, Yamaoka and Tsuji [7-9] have investigated the structure of a rich fuel-air flame in the forward stagnation region of a porous cylinder. Their work improves understanding of two-stage combustion. Yamaoka and Tsuji indicated that, as the equivalence ratio decreases, the premixed flame approaches the porous cylinder which results in considerable heat loss from the flame through heat conduction to the burner and radiation from it. This heat loss complicates the boundary conditions for numerical simulation. In addition, because of the porous cylinder, it is difficult to add sprays into the Tsuji burner. Therefore, this attractive geometry is not employed here.

The NO_x emission characteristics of methane-air combustion in two-stage flames of Yamaoka and Tsuji [7-9] were studied numerically by Nishioka et al. [10] who used a chemical-kinetic data base given by Miller and Bowman [11] in 1989, which included 235 steps and 52 species. The results of their nu-

Downloaded from http://asmedigitalcollection.asme.org/GT/proceedings-pdf/GT1996/78743/V003T06A053/2407413/v003t06a053-96-gt-545.pdf by gues

merical integrations showed that the maximum NO emission index was smaller than 1 g/kg-CH_4 when the equivalence ratio was in the range of 1.5 to 3.0 with strain rates less than 50 s^{-1}. They also found that the prompt NO and thermal NO contributed almost equally to the NO emission index. Since an improved chemical-kinetic data base is now available, it is useful to see how different the results can be by using different chemical-kinetic data bases.

EXPERIMENT

Experimental Arrangement

A two-phase laminar counterflow burner is employed in the present study. As shown in Fig.1, fuel-rich methane-air mixtures flow through the upper duct and the water spray, produced by a pressure atomizer, is carried by air through the lower duct. Both ducts have the same exit radius of 22.5 mm. The separation distance between the upper and lower ducts is $L = 18$ mm. The other details of the experimental arrangement have been described earlier [12-13]. With this burner, a well-defined laminar two-stage flame can be obtained, as shown in the photograph in Fig.1. Gas chromatographic analysis shows that methane is consumed in the premixed flame and produces hydrogen and carbon monoxide that burn in the diffusion flame, which is stabilized near the stagnation plane, as illustrated in the figure.

In the present experiment, the flame structure is controlled by the equivalence ratio of the methane-air mixture in the top stream and by the strain rate of the counterflowing streams. The former is determined by the ratio of Q_F, the volumetric flow rate of methane, to Q_+, the total volumetric flow rate of the methane-air mixture, while the latter is determined by both Q_+ and Q_-, the total flow rate of the air stream directed against the methane-air stream. The ratio Q_+/Q_- controls the location of the flame between the two duct exits. There are only three experimentally adjustable parameters, Q_+, Q_F and Q_-, because the volumetric flow rate of the water spray is a function of Q_-, as discussed previously [12]. Three flowmeters are used in the present study to measure Q_+, Q_F and Q_-. In our experiment, the ratio of Q_F/Q_+ is adjusted so that the equivalence ratio is in the range from 1.3 to 3.0. The strain rate is established in the range from 50 to 250 s^{-1} by adjusting Q_+ and Q_-. It is found experimentally that when $Q_+/Q_- \approx 1$, the light blue diffusion flame can be stabilized at a position approximately equidistant from the two duct exits, and this is the condition selected for the experiments, to minimize flame interactions with the ducts.

Experimental Diagnostics

The species H_2, O_2, N_2, CH_4, CO, CO_2, C_2H_2, C_2H_4 and C_2H_6 are measured by a Varian 3600 gas chromatograph (Varian Instrument Group) that has molecular sieve and porapak-Q columns with a thermal conductivity detector. A Varian DS-651 data system (Varian Instrument Group) is used to control the gas chromatograph and to perform the data analysis. High-purity helium is employed as the carrier gas flowing in the columns and as the reference gas. The quartz micro-sampling probe employed was a standard type, as described by Fristrom and Westernberg [14] and by Saito et al.[15], and it is mounted on an r-z positioner to fix the probe at the desired location. The inner diameter of the probe tip is smaller than 0.1 mm. Samples are withdrawn from the flame continuously at a line pressure of 0.6 atm, monitored by an electronic pressure transducer. Since this transducer does not have room to accumulate gas, the sample volume needed in the measurement is significantly reduced, compared with a mechanical vacuum pressure gauge. In the measurement, as long as the sampling line pressure is the same, the values of peak area are very repeatable for all the species ex-

Downloaded from http://asmedigitalcollection.asme.org/GT/proceedings-pdf/GT1996/78743/V003T06A053/2407413/v003t06a053-96-gt-545.pdf by guest

cept H_2O. The well-known difficulty with H_2O is due to water condensation in the sampling system and to interaction of water vapor with the material in the columns. The problem is greatest when samples are taken from the flame zone where water concentrations are high. In the data analysis, we assume that the water concentration in the flame zone is a known parameter which is given by the numerical computation. Since air contains 0.932% argon, which elutes with oxygen, the results for oxygen are corrected to account for argon by use of the measured concentration of nitrogen.

Centerline temperature profiles in the present two-stage flame are measured by a Pt-6%Rh vs. Pt-30%Rh thermocouple with a bead diameter of 135μm. Corrections for radiation are made based on available literature[16]. Although the two-stage flame is very flat over a circle with diameter equal to the diameter of the duct exit, the flame curves up at the edges because of the exhaust ventilation (see photograph in Fig.1). When the thermocouple is positioned between the the upper duct exit and the premixed flame, the curved flame outside of the duct heats the thermocouple extension, and heat conduction from the extension to the bead is not negligible so that the temperature measurement in that region becomes inaccurate. In the present paper, we therefore do not report the results of temperature measurements in that region.

Velocity fields and spray structure are measured by a two-component fiber-optical phase-doppler particle analyzer(PDPA) that has been discussed previously [13]. The probe volume formed by the laser beams of the PDPA is positioned at the desired point by moving the burner assembly axially and radially. Data on the arrival time, velocity and diameter of droplets passing through the probe volume are then recorded by collecting about 4000 samples at each probe position.

The flame configurations are recorded by a camera, and the separation distance between the premixed and diffusion flames is measured on the photograph. A thin laser sheet is constructed by directing a 2W argon-ion laser beam (wavelength 488 nm) through cylindrical lenses to observe the relative position of the vaporization plane of the water spray, with respect to the flame location. Trajectories of the water droplets in the spray stream, illuminated by the laser sheet, are recorded by a camera. These photographs provide useful information in interpreting the experimental results obtained by the PDPA.

Analysis of the flow-visualization and PDPA data gives droplet trajectories, droplet number densities and evaporation rates. These experimental results, along with the measured profiles of temperature and species concentrations, can be compared with results of numerical computations.

NUMERICAL INTEGRATIONS

The numerical integrations apply to laminar flames with potential flow in the outer streams. Only the radiation from CO, CO_2 and H_2O is taken into account in the energy equation. In accounting for water addition, single-phase flow was assumed throughout the computational domain for simplicity, but the heat of vaporization of water is taken into account in the energy equation. With these assumptions, the equations of continuity, r-direction momentum, energy and chemical species essentially reduce to those given previously [5,6], with the air-side external strain rate a as a constant parameter. For the present problem, the boundary conditions are

$$Y_{CH_4} = Y_{CH_4-\infty},\ Y_{O_2} = Y_{O_2-\infty} = 4Y_{CH_4-\infty}/\Phi,$$
$$Y_{N_2} = Y_{N_2-\infty} = 3.3Y_{O_2-\infty},\ Y_i = 0, \text{ otherwise}$$
$$T = 298K,\quad \rho w = \rho_{-\infty} w_{-\infty} \quad \text{at } z = -L_s;$$
$$Y_{O_2} = Y_{O_2\infty},\ Y_{N_2} = Y_{N_2\infty} = 3.3Y_{O_2\infty},$$
$$Y_{H_2O} = Y_W,\ Y_i = 0, \text{ otherwise}$$
$$T = 298K,\ \rho w = \rho_\infty w_\infty \quad \text{at } z = L_s.$$

Downloaded from http://asmedigitalcollection.asme.org/GT/proceedings-pdf/GT1996/78743/V003T06A053/2407413/v003t06a053-96-gt-545.pdf by guest

The present reaction mechanism consists of 140 elementary steps most of which are reversible. The rate coefficients of 55 reactions related to the C_1 and C_2 chemistry come from a recent publication (namely, reactions 1-18, 21-24 and 29-61 in Table 1 of [17]). The rate data for the other 85 reactions, related to CH, $^3CH_2$, $^1CH_2$ and NO_x formation, are essentially the same as those given in [18] but updated by Hewson et al. [19]. The following 38 species are involved in chemical scheme: CH_4, O_2, CO, CO_2, H_2, H_2O, H, OH, O, HO_2, H_2O_2, CH, CHO, CHCO, $^1CH_2$, $^3CH_2$,CH_2O, CH_3, C_2H, C_2H_2, C_2H_3, C_2H_4, C_2H_5, C_2H_6, N, NH, NH_2, NH_3, NO, HNO, HCN, HNCO, NCO, CN, NO_2, N_2, N_2H, N_2O.

The present numerical computations are performed employing a numerical code developed at RWTH, Aachen, Germany [20]. The method of solution implemented in the code is essentially the same as in an older code [5,6,21]. This code was modified locally to include the effects of droplet vaporization in the energy equation. In the present paper, we report results for a strain rate of 100 s^{-1} at atmospheric pressure. The equivalence ratio is varied from Φ =1.3 to Φ =3.0. For each value of Φ, the water mass fraction Y_W in the air stream is changed from 0 to 15% in the calculations.

RESULTS

Droplet Velocity and Spray Structure

Experimentally, the stagnation plane is always located in the light blue region of the diffusion flame when Φ is in the range from 1.3 to 3.0 and the strain rate is in the range from 50 to 250 s^{-1}, although the stagnation plane may not completely coincide with the center of the blue region. For convenience, the light blue diffusion flame is set in the center plane between two exits by adjusting Q_- and the stagnation plane can be assumed to be nearly midway between the duct exits. As shown in Fig.1, the origin of the $z-r$ coordinates is at the center of the stagnation plane, with $z = L_s$ at the air-spray exit and $z = -L_s$ at the methane-air exit. In this coordinate system, particles moving upward have negative velocity and vise versa.

Different initial flow conditions are studied to obtain different strain rates in the counterflow streams, but in the present paper the main condition discussed has Q_+=870 cm^3/s and Q_-=850 cm^3/s. The local strain rates on the burner axis are determined based on the PDPA measurement. We first plot the measured axial velocity as a function of the coordinate z and fit a curve to the data to define the air-side strain rates as $a = -dw/dz$. With the flow condition given here, $a = 100\ s^{-1}$.

Figure 2 shows the spray structure for an equivalence ratio of 1.4. For convenience, the number density, Sauter mean diameter and liquid volume flux are normalized by 18800 cm^{-3}, 38μm and 0.0035 cm^3/cm^2-s, respectively. The axial velocity w_p is shown as open circles, while other symbols represent normalized number density, Sauter mean diameter, and liquid volume flux. The results in this figure are what one would expect for counterflow streams with the flame present. The Sauter mean diameter becomes larger in the neighborhood of the vaporization plane because smaller droplets move away from the stagnation streamline in the radial direction more easily and vaporize faster.

Figure 3 compares the profiles of axial velocity for a strain rate of 100 s^{-1}. The points are measured mean axial velocities of droplets smaller than 5 μm, which we take as a measure of the gas velocity, since small droplets are expected to follow the gas. To assist in understanding how the flame affects the velocity field, the predicted temperature profiles are plotted in the figure as well. Agreement is good where data exist. Where droplets are absent, the computed velocity profiles differ considerably for the two values of Φ.

Downloaded from http://asmedigitalcollection.asme.org/GT/proceedings-pdf/GT1996/78743/V003T06A053/2407413/v003t06a053-96-gt-545.pdf by g

Flame Structure

The separation distance between the premixed flame and the diffusion flame at a given strain rate strongly depends on Φ. Figure 4 illustrates how the measured distance between the two flames changes with changing equivalence ratio. It indicates that the separation distance increases with decreasing Φ. Figure 4 also indicates the predicted distances between the concentration peaks of OH and C_2H_4 and those of OH and CH. It shows that the former is larger than the latter although they become nearly equal for $\Phi < 1.5$. The measured distance is closer to the predicted distance between the concentration peaks of OH and C_2H_4, suggesting that the green emissions come not from CH but rather from species involved in C_2H_4 formation.

Figures 5a and 5b for $\Phi = 1.35$ and Figs.6a and 6b for $\Phi = 2.20$ show profiles of temperature measured by thermocouple and concentrations measured by gas chromatography. The agreement between experiment and numerical computation is very good for temperature and for most of the species measured. There is some quantitative disagreement between experiment and theoretical prediction for X_{H_2} in Fig.5a, but even these agree better than a factor of two.

We see from Fig.5 that methane and oxygen in the rich mixture react very rapidly to form CO and H_2, and X_{CO} and X_{H_2} reach maxima as X_{CH_4} becomes zero. The further oxidation of CO and H_2 to form CO_2 and H_2O occurs in the diffusion flame. The C_2 species, such as C_2H_2, C_2H_4 and C_2H_6 are produced rapidly as CH_4 disappears. However these species have very short lives, and they cannot be found experimentally in the diffusion flame in Fig.5. Figures 5b and 6b clearly show that the concentrations of C_2 species strongly depend on the equivalence ratio; the richer the flame is, the higher is the concentration of C_2 species, consistent with observed soot emissions in fuel-rich methane-air flames. Since the computations here overpredict X_{C_2}, the reaction mechanism needs some revision to be consistent with the experimental results.

Since radicals such as H, OH and O play dominant roles in hydrocarbon flames, knowledge of their distributions in the flame should help in understanding flame structure and NO_x formation. Figures 7a and 7b show predicted profiles of concentrations of H, OH and O, for Φ =1.35 and 2.20, respectively. The separation of peaks for $\Phi = 1.35$ means that two flames are present, while for $\Phi =$ 2.20 they have merged into one. To give further information on minor fuel species, X_{CH_3} and and X_{C_2}, which includes C_2H_2, C_2H_4 and C_2H_6, are also plotted. Both peak in the premixed flame. It is found that the maximum concentrations of CH_3, $^3CH_2$, $^1CH_2$ and CH are of order 10^{-3}, 10^{-5}, 10^{-6} and 10^{-6}, respectively, while those of C_2H_2, C_2H_4, C_2H_6, C_2H_5, C_2H_3, and C_2H are of order $5x10^{-3}$, $2x10^{-3}$, $2x10^{-3}$, 10^{-5}, 10^{-5}, 10^{-6}, respectively.

INFLUENCE OF WATER ADDITION ON NO_x FORMATION

Influence of Water Addition on the Prompt Mechanism

Since the prompt NO formation begins with the reaction $CH + N_2 \rightleftharpoons HCN + N$ as found by Fenimore [22], it is helpful to understand how the species in this reaction are distributed in the flame zone and how the temperature and water concentration affect them. Figures 8a, 9a and 10a show concentration profiles of CH, N and HCN without water added, respectively, while Figs.8b, 9b, and 10b show distributions of these species with $Y_W = 10\%$ water added in the air stream. In these figures, Φ changes from 1.35 to 3.00, and profiles of temperature corresponding to each Φ are also plotted for reference.

According to Fig.8a, without water, the peak concentration of CH is high at Φ =1.35, decreases to its lowest value at Φ =1.5 then increases to a

Downloaded from http://asmedigitalcollection.asme.org/GT/proceedings-pdf/GT1996/78743/V003T06A053/2407413/v003t06a053-96-gt-545.pdf by gu

large value at Φ =3.0. As shown in Fig.8b, the water addition in the air stream significantly reduces the CH concentration when Φ is larger than 1.7 but has little influence on CH when Φ is smaller than 1.55. It is found that the concentrations of CH are directly controlled by the reactions

1 $CH + H_2O \rightleftharpoons CH_2O + H$

2 $CH + O_2 \rightleftharpoons CHO + O$

3 $CH + CO_2 \rightleftharpoons CHO + CO$

4 $^3CH_2 + H \rightleftharpoons CH + H_2$

5 $^3CH_2 + OH \rightleftharpoons CH + H_2O$

where the first three consume CH and the last two produce it. It is clear that when the premixed flame is close to the diffusion flame ($\Phi \geq 1.7$), the CH production can be slowed significantly by increasing water concentration in the air stream. When the premixed flame is far from the stagnation plane, the water added in the air stream cannot reach the region where CH is produced. As expected, the reaction $CH + N_2 \rightleftharpoons HCN + N$ is unimportant for the CH concentration because it is much slower than reactions 1 to 3.

When Φ is relatively high, water addition in the air stream seems to greatly reduce the concentration of the radical N, as illustrated in Figs.9a and 9b. For example, with Φ =3.0, the maximum value of X_N is about 10^{-7} with water addition, while it is about $6x10^{-7}$ without water addition. Of importance for N are

6 $N_2 + CH \rightleftharpoons N + HCN$

7 $NH + H \rightleftharpoons N + H_2$

8 $NH + OH \rightleftharpoons N + H_2O$

9 $NCO + M \rightleftharpoons N + CO + M$

10 $N + OH \rightleftharpoons NO + H$

11 $N + O_2 \rightleftharpoons NO + O$

where reactions 6 through 9 produce N, while 10 and 11 consume it. The calculations show that reaction 6 contributes most to the production of N, while reaction 10 is much faster than reactions 11 in consuming N. Reaction 6 slows down when X_{CH} decreases. From these discussions, we can see that most of the N produced here comes from the prompt mechanism.

The species HCN is an important intermediate in NO_x production. As indicated in Figs.10a and 10b, its concentration strongly depends on the flame structure and water addition in the air stream. Reactions for X_{HCN} are

6 $N_2 + CH \rightleftharpoons N + HCN$

12 $NO + CH \rightleftharpoons O + HCN$

13 $HCN + O \rightleftharpoons NCO + H$

14 $HCN + H \rightleftharpoons CN + H_2$.

The HCN is produced by the first two reactions and is consumed by the last two. At lower equivalence ratios, reaction 6 plays a more important role in the production of HCN, while 12 is more important at high equivalence ratios. Water addition reduces HCN by reducing CH concentrations in both reactions 6 and 12. Whether HCN yields NO or N_2 depends on the oxidation of NCO and CN.

Influence of Water Addition on the Emission Index

The NO emission index by reaction j is defined as

$$E_j = \frac{\int_{-L_s}^{L_s} M_{NO}\, \dot{\omega}_{NO_j}\, dz}{-\int_{-L_s}^{L_s} M_{CH_4}\, \dot{\omega}_{CH_4}\, dz},$$

where $-\dot{\omega}_{CH_4}$ is the total consumption rate of methane. The total NO emission index is defined by

$$E = \Sigma_j E_j.$$

According to these definitions, some of the E_j are negative, describing "reburn" of NO.

Figure 11 illustrates the emission index E_j contributed by various reactions. Several conclusions

Downloaded from http://asmedigitalcollection.asme.org/GT/proceedings-pdf/GT1996/78743/V003T06A053/2407413/v003t06a053-96-gt-545.pdf by guest

are suggested from this figure. First, NO formation is dominated by the prompt mechanism, since the thermal NO reactions 11 and 19 are not important and since the N atom in reaction 10 is mainly produced by the reaction $CH + N_2 \rightleftharpoons HCN + N$, as discussed previously. Second, E_j for a specific reaction j may be much higher than E because of NO consumption. For instance, E_{16}, is about 3 g/kg-CH_4, while E is only 1.8 g/kg-CH_4 for Φ =3.0 without water addition. This suggests strategies for reducing the NO_x formation by slowing down the reactions that contribute most to NO formation. Third, water addition in the air stream can greatly affect E at large Φ.

The role of water addition in reducing the emission index can be understood by studying Figs.12a and 12b. Comparison can be made between profiles of X_{NO} without water added, as shown in Fig.12a, and those with water added in the air streams, as shown in Fig.12b. We see that concentrations of NO increase with increasing Φ without added water, and the concentration peaks become substantially smaller when water is added. Results in these two figures indicate that the NO formation strongly depends on the flame structure and on the water concentration in the flame.

Figure 13 plots the predicted E as a function of Φ and Y_W at a strain rate of 100 s^{-1}. It can be seen that when Y_W =0, E decreases slightly and then increases as Φ increases from 1.36 to 3.00. As Y_W increases, E decreases, and the water addition is always more effective in reducing NO_x when Φ is large.

The NO_x emission index is very sensitive to the rate parameters for the reaction $CH + N_2 \rightarrow HCN + N$. The most direct determination of those parameters is the shock-tube study of Dean et al. [23] and from the experimental results, the rate constant is found to be $k = 4.4\times10^{12} \exp(-11072/T)$ cm^3/mole-s. With this rate, the NO_x emission predicted by the present study is higher than that predicted by Nishioka et al.[10], who used a lower rate constant. Measurements of NO_x in these flames would be desirable to test these predictions.

CONCLUSIONS

Well-defined two-stage flames in counterflowing streams have been employed in testing a chemical-kinetic data base for H-C-N-O combustion systems recently published. Agreement between measured and predicted profiles of temperature and CO, CO_2, CH_4 and O_2 is very good. The present computation overpredicts the concentrations profiles of C_2H_2, C_2H_4 and C_2H_6 and thus suggests that the reaction mechanism needs to be revised in the future. Flame visualization and PDPA measurements indicate that water droplets in the air-spray stream very rapidly disappear through vaporization at the vaporization plane, which is close to the diffusion flame. The water vapor from the spray helps to increase the water concentration in flame zone. Numerical computations reveal that prompt NO in the present two-stage counterflow combustion plays a dominant role in NO_x formation and that the NO_x emission index strongly depends on the flame structure and on the mass fraction of water added in the air stream. The NO_x emission index can be substantially reduced by adding water to remove CH.

ACKNOWLEDGMENT

We are indebted to R.X. Zang and W. Willemse of UCSD for helping with experimental measurement and to M. Bollig of RWTH, Aachen, Germany for helping with numerical computation. This research was supported by the Department of Energy, Office of Basic Energy Sciences, Division of Engineering and Geosciences under contract DE-F003-87ER13685.

Downloaded from http://asmedigitalcollection.asme.org/GT/proceedings-pdf/GT1996/78743/V003T06A053/2407413/v003t06a053-96-gt-545.pdf by guest

REFERENCES

1 Yamagishi, K., Nozawa, M., Yoshie, T., Tokumoto, T. and Kakegawa, Y., "A Study of NO_x Emission Characteristics in Two Stage Combustion," *Fifteenth Symposium (International) on Combustion,* The Combustion Institute, Pittsburgh, 1975, pp.1157-1166.

2 Becker, B., Berenbrink, P. and Brandner, H., "Premixing Gas and Air to Reduce NO_x Emissions with Existing Proven Gas Turbine Combustion Chambers," Paper No. B-9, Presented at the International Gas Turbine Conference and Exhibit, Dusseldorf, West Germany, June 8-12, 1986.

3 Howe, G.W., Li, Z., Shih, T.I-P., and Nguyen, H.L., "Simulation of Mixing in the Quick Quench Region of a Rich Burn-Quick Quench Mix-lean Burn Combustor," AIAA Paper 91-0410, January, 1991.

4 Seshadri, K., Puri, I.K. and Peters, N., "Experimental and Theoretical Investigation of Partially Premixed Diffusion Flames at Extinction," *Combustion and Flame*, Vol.61, 1985, pp.237-249.

5 Smooke, M.D., Seshadri, K. and Puri, I.K., "The structure and Extinction of Partially Premixed Flames Burning Methane in Air," *Twenty-Second Symposium (International) on Combustion,* The Combustion Institute, Pittsburgh, 1988, pp.1555-1563.

6 Smooke, M.D., Crump, J., Seshadri, K. and Giovangigli, V., "Comparison between Experimental measurements and Numerical Calculations of the Structure of Counterflow, Diluted, Methane-Air, Premixed Flames," *Twenty-Third Symposium (International) on Combustion,* The Combustion Institute, Pittsburgh, 1990, pp.463-470.

7 Yamaoka, I., and Tsuji, H., "The Structure of Rich Fuel-Air Flames in the Forward Stagnation region of a Porous Cylinder," *Fifteenth Symposium (International) on Combustion,* The Combustion Institute, Pittsburgh, 1975, pp.637-644.

8 Yamaoka, I., and Tsuji, H., "Structure Analysis of Rich Fuel-Air Flames in the Forward Stagnation region of a Porous Cylinder," *Sixteenth Symposium (International) on Combustion,* The Combustion Institute, Pittsburgh, 1977, pp.1145-1154.

9 Yamaoka, I., and Tsuji, H., "An Experimental Study of Flammability Limits Using Counterflow Flames," *Seventeenth Symposium (International) on Combustion,* The Combustion Institute, Pittsburgh, 1979, pp.843-855.

10 Nishioka, M., Nakagawa, S., Ishikawa, Y., and Takeno, T., "NO Emission Characteristics of Methane-Air Double Flame," *Combustion and Flame*, Vol.98, 1994, pp.127-138.

11 Miller, J.,A. and Bowman, C.T., "Mechanism and Modeling of Nitrogen Chemistry in Combustion," *Prog. Energy Combust. Sci.*, Vol.15, 1989, pp.287-338.

12 Li, S.C., Libby, P.A. and Williams, F.A., "Experimental and Theoretical Studies of Counterflow Spray Diffusion Flames," *Twenty-Fifth Symposium (International) on Combustion*, The Combustion Institute, Pittsburgh, 1992, pp.1503-1512.

13 Li, S.C., Libby, P.A., and Williams,F.A., "Spray Structure in Counterflowing Streams with and without a Flame," *Combustion and Flame*, vol.94, pp. 1993, 161-177.

14 Fristrom, R.M. and Westernberg, A.A. *Flame Structure*, McGraw-Hill, New York, 1965.

Downloaded from http://asmedigitalcollection.asme.org/GT/proceedings-pdf/GT1996/78743/V003T06A053/2407413/v003t06a053-96-gt-545.pdf by guest

15 Saito, K., Williams, F.A. and Gordon, A.S., "Structure of Laminar Coflow Methane-Air Diffusion Flames," *J. Heat Transfer*, Vol.108, P640, 1986.

16 Sato, A., Hashiba, K., Hasatani, M., Sugiyama, S. and Kimura, J., "A Correctional Calculation Method for Thermocouple Measurements of Temperatures in Flames," *Combustion and Flame*, Vol.24, 1975, pp.35-41.

17 Peters, N., "Flame Calculations with Reduced Mechanism-an Outline," in *Reduced Kinetic Mechanisms for Applications in Combustion Systems* (N. Peters and B. Rogg, Eds.), Spinger-Verlag, Berlin, 1993, pp.3-13.

18 Bockhorn, H., Chevalier, C., Warnatz, J. and Weyrauch, V., "Experimental Investigation and Modeling of Prompt-NO Formation in Hydrocarbon Flames," in *Heat Transfer in Fire and Combustion Systems*, HTD-Vol.166, American Society of Mechanical Engineers, 1991, pp.11-16.

19 Hewson, J.C., Bollig, M., "Reduced Mechanisms for NO_x Emissions from Hydrocarbon Diffusion Flames," submitted to *Twenty-sixth Symposium (International) on Combustion*, The Combustion Institute, Pittsburgh, 1996,

20 Pitsch, H., *Entwicklug eines Programmpaketes zur Berechnung eindimensionaler Flammen am Beispiel einer Gegenstomdiffusionsflamme.* Master thesis, RWTH Aachen, Germany, 1993.

21 Smooke, M.D, Miller, J.A., Kee, R.J., "Solution of Premixed and Counterflow diffusion Flame Problems by adaptive Boundary Value Methods," *Numerical Boundary Value ODEs*, edited by U.M. Ascher and R.D. Russel, Birkhöuser Boston Inc. pp.303-317, 1985.

22 Fenimore, C.P., "Formation of Nitric Oxide in Premixed Hydrocarbon Flames" *Thirteenth International Symposium on Combustion*, The Combustion Institute, Pittsburgh, 1971, pp.373-379.

23 Dean, A.J., Davidson, D.F., Hanson, R.K. and Bowman, C.T., "Development and Application of CH Laser Absorption diagnostic for Shock Tube Kinetic Studies," *Western States Section/Combustion Institute Meeting*, Paper No. 88-91 (1988).

Downloaded from http://asmedigitalcollection.asme.org/GT/proceedings-pdf/GT1996/78743/V003T06A053/2407413/v003t06a053-96-gt-545.pdf by guest

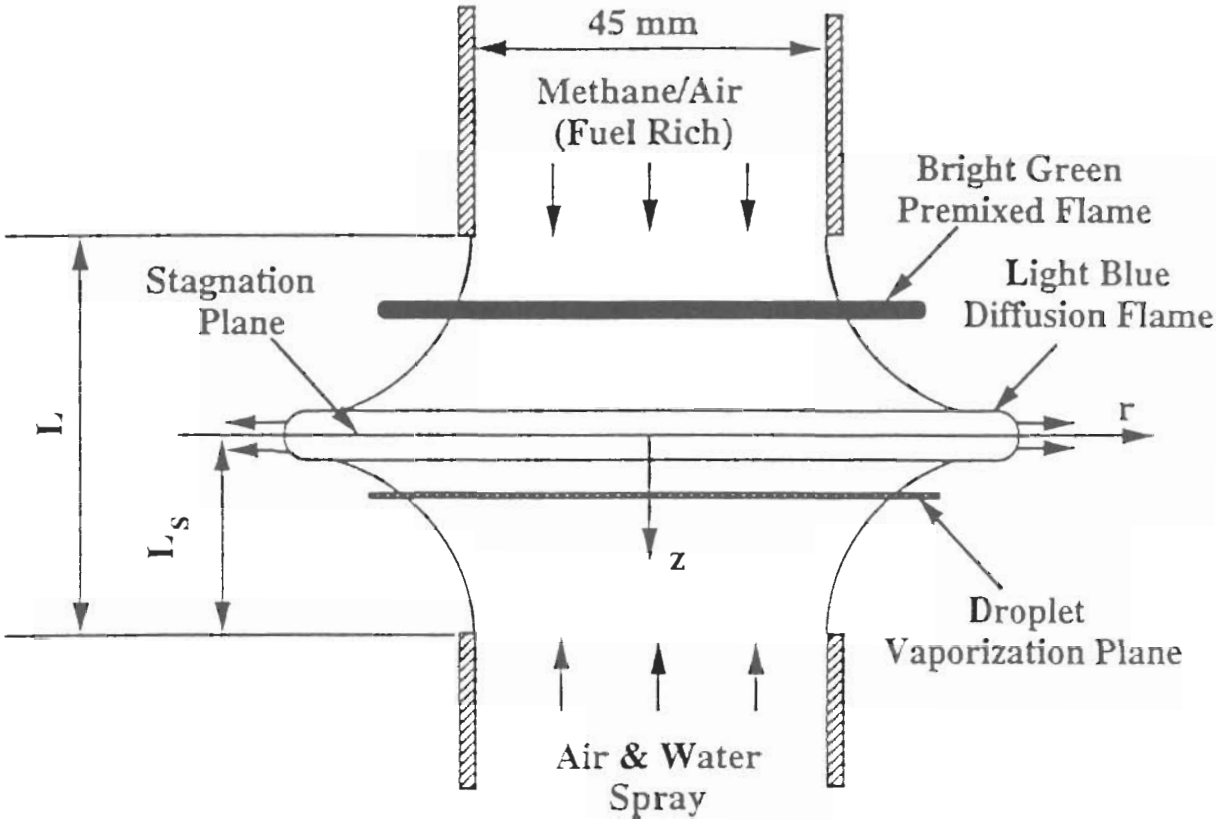

Fig.1a: Sketch of a two-stage methane-air flame in water-spray counterflowing streams.

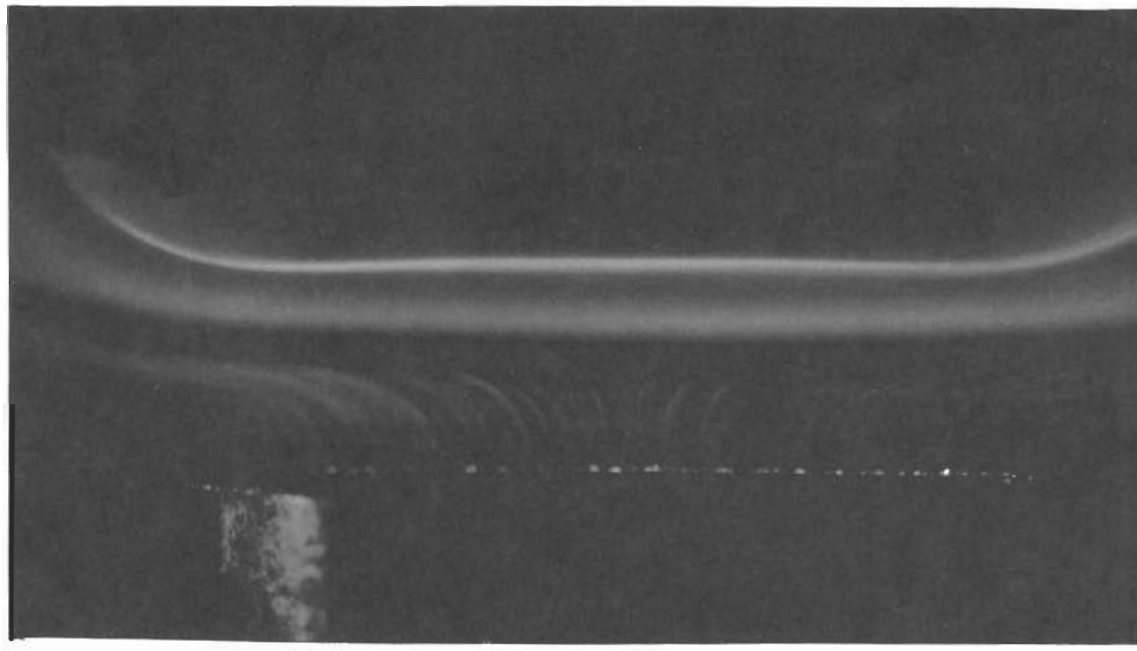

Fig.1b: A photograph of the flame sketched above.

Downloaded from http://asmedigitalcollection.asme.org/GT/proceedings-pdf/GT1996/78743/V003T06A053/2407413/v003t06a053-96-gt-545.pdf by gue

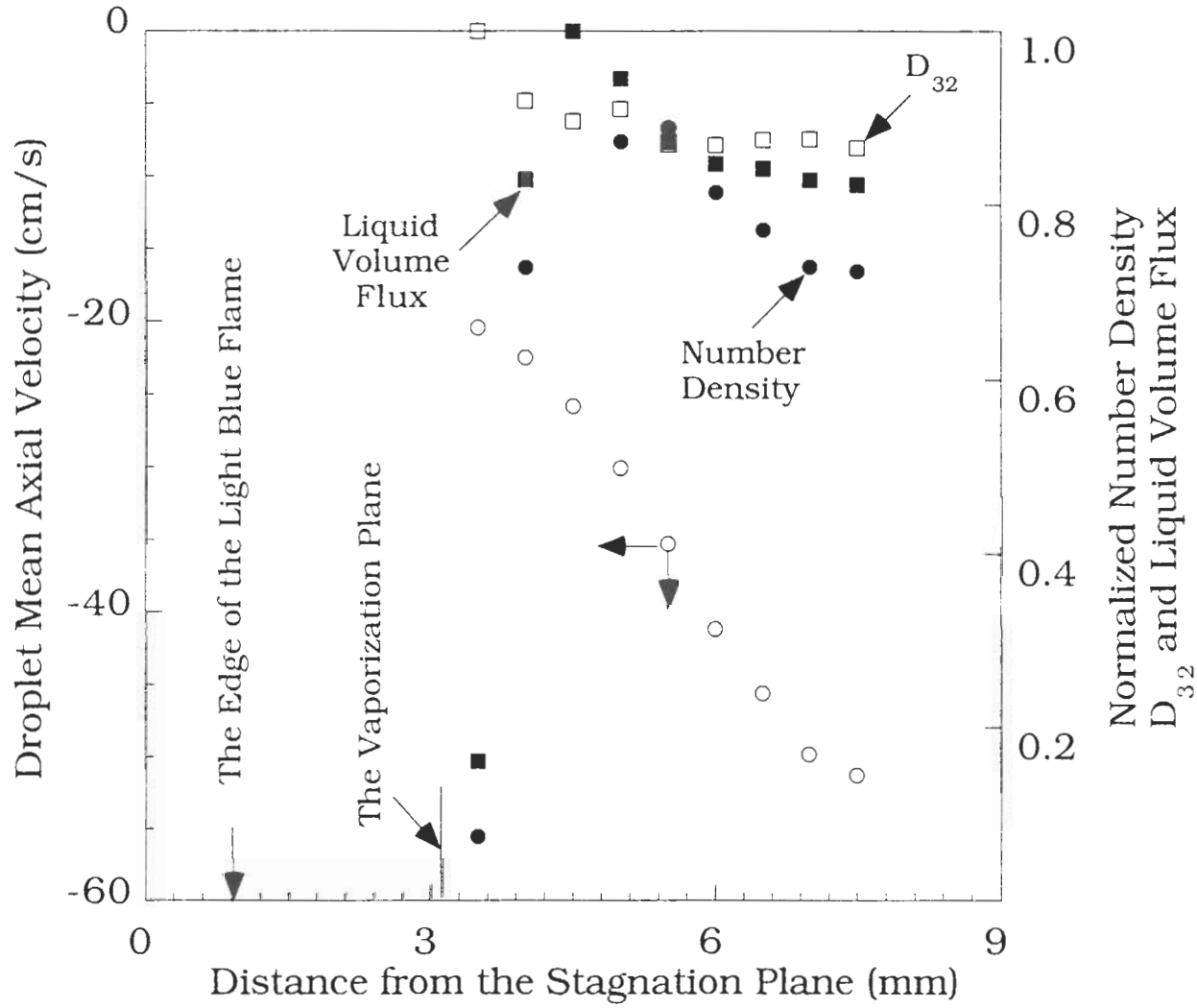

Fig.2: Measured droplet axial velocity, number density, Sauter mean diameter and liquid volume flux on the burner axis (the last three variables are normalized by their maximum values).

Downloaded from http://asmedigitalcollection.asme.org/GT/proceedings-pdf/GT1996/78743/V003T06A053/2407413/v003t06a053-96-gt-545.pdf by guest

Fig.3: Comparison between measurement and prediction of profiles of axial velocity.

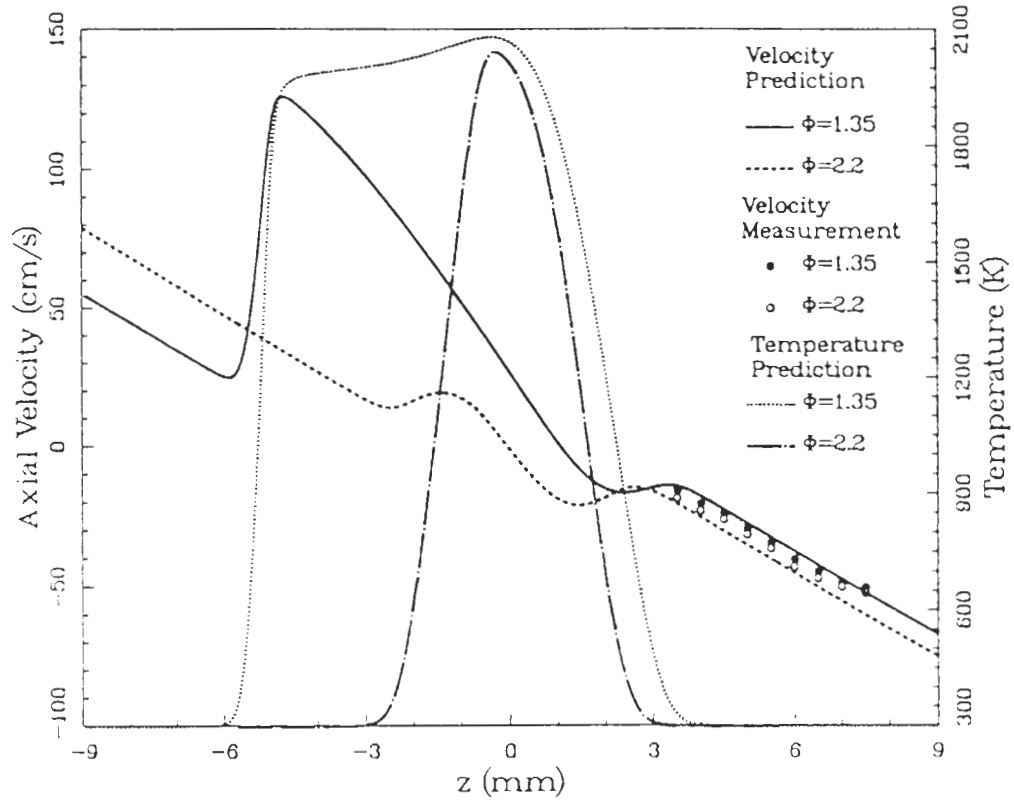

Fig.4: Comparison of measured distance between two luminous flames with predicted distances between the concentration peaks of CH and OH and of C_2H_4 and OH.

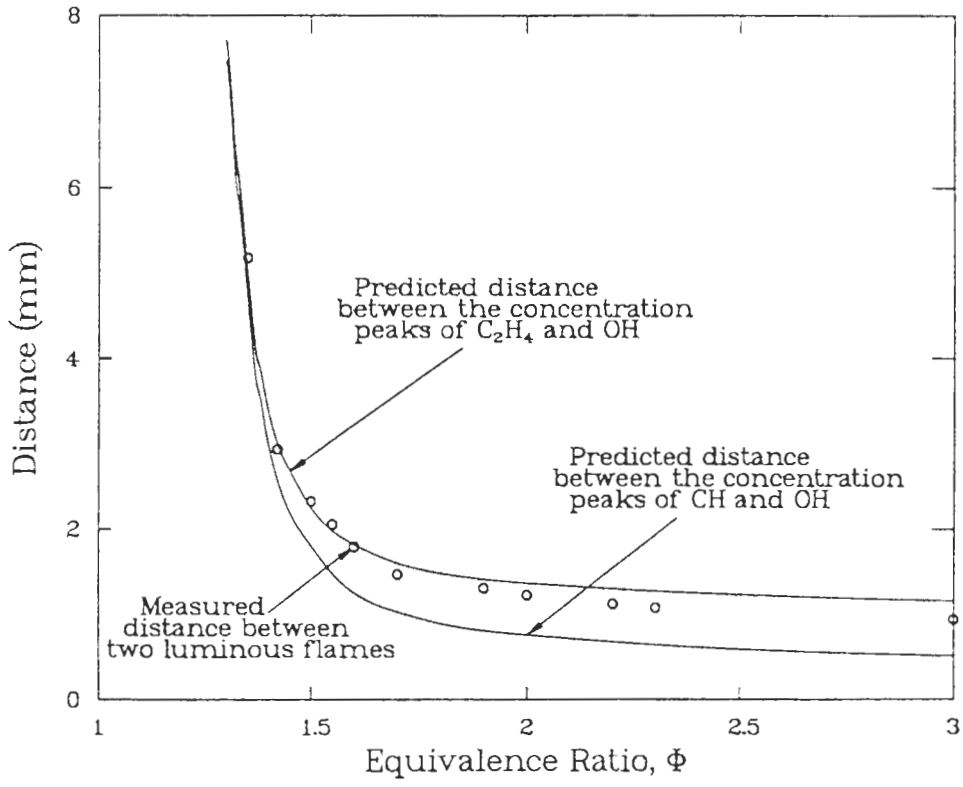

Downloaded from http://asmedigitalcollection.asme.org/GT/proceedings-pdf/GT1996/78743/V003T06A053/2407413/v003t06a053-96-gt-545.pdf by gue

Fig.5a: Comparison between measurement and prediction for concentration profiles for Φ=1.35 without water.

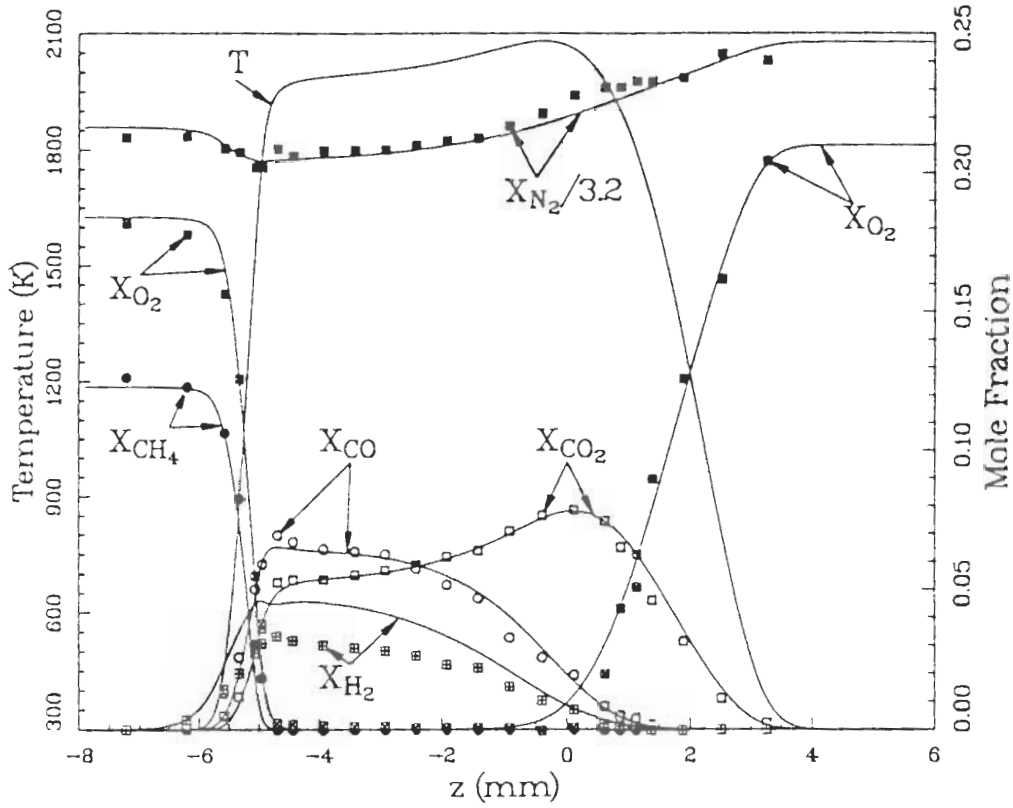

Fig.5b: Comparison between measurement and prediction for profiles of temperature and of the sum of the mole fractions of C_2H_2, C_2H_4 and C_2H_6 for Φ=1.35 without water.

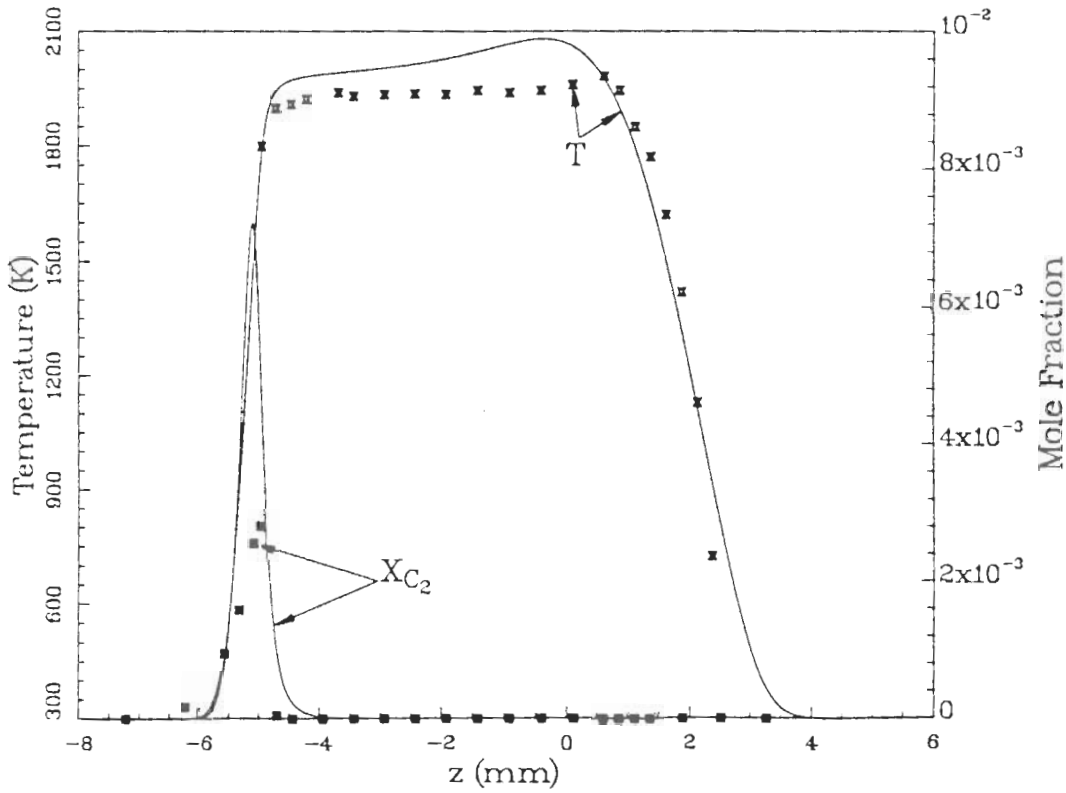

Downloaded from http://asmedigitalcollection.asme.org/GT/proceedings-pdf/GT1996/78743/V003T06A053/2407413/v003t06a053-96-gt-545.pdf by

Fig.6a: Comparison between measurement and prediction for concentration profiles for Φ=2.20 without water.

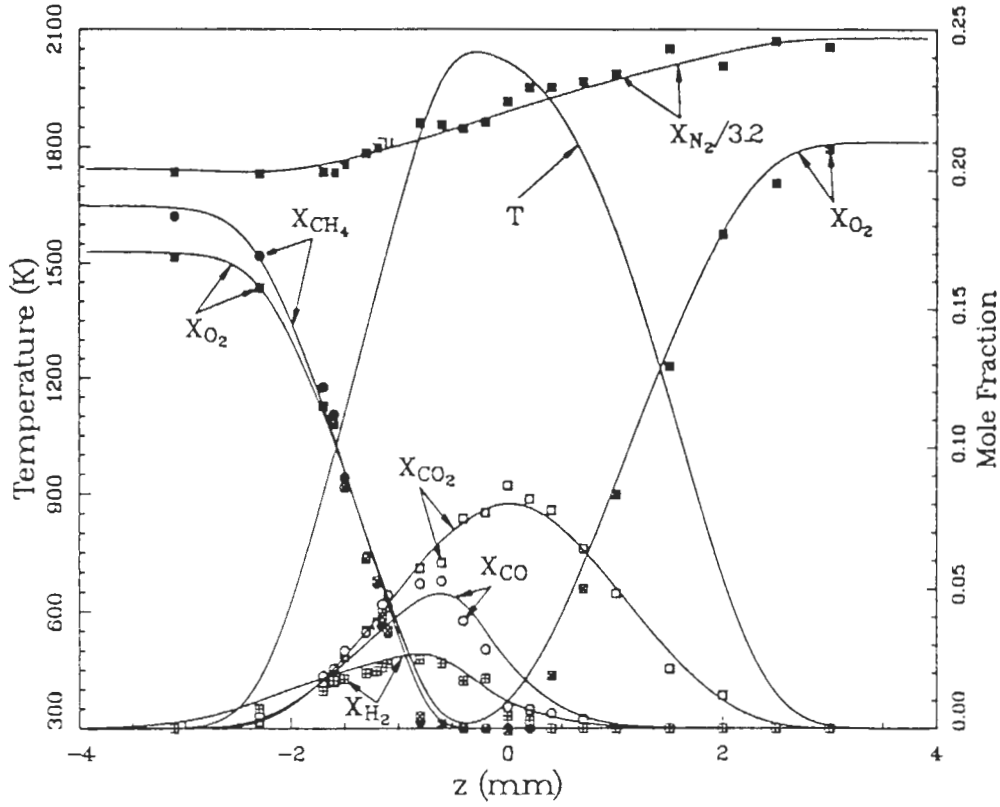

Fig.6b: Comparison between measurement and prediction for profiles of temperature and of the sum of the mole fractions of C_2H_2, C_2H_4 and C_2H_6 for Φ=2.20 without water.

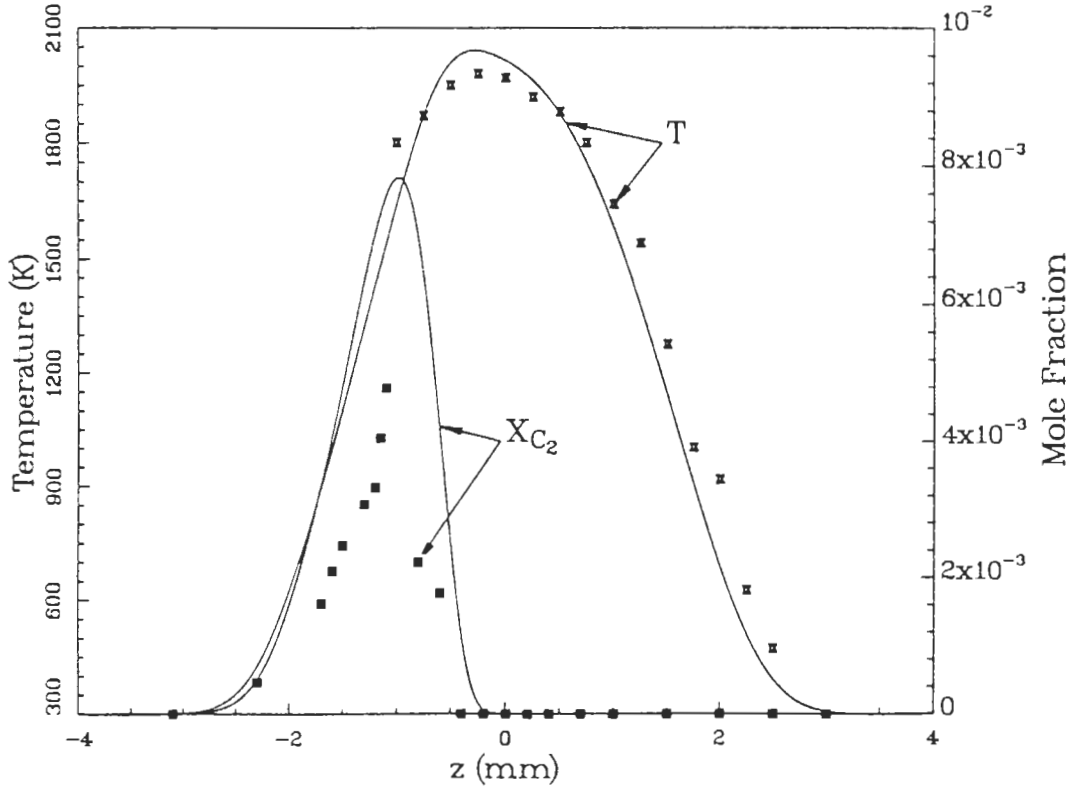

Downloaded from http://asmedigitalcollection.asme.org/GT/proceedings-pdf/GT1996/78743/V003T06A053/2407413/v003t06a053-96-gt-545.pdf by gue

Fig.7a: Predicted profiles of temperature and radical concentration for Φ=1.35.

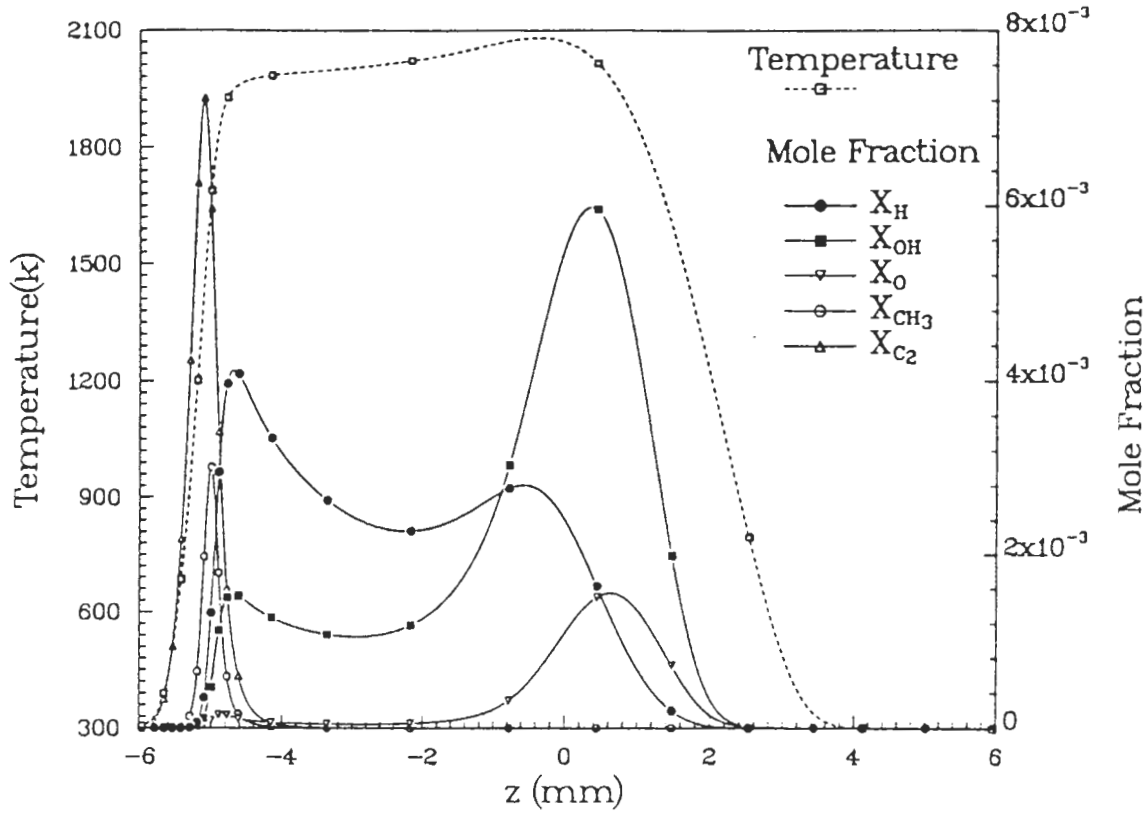

Fig.7b: Predicted profiles of temperature and radical concentration for Φ=2.20.

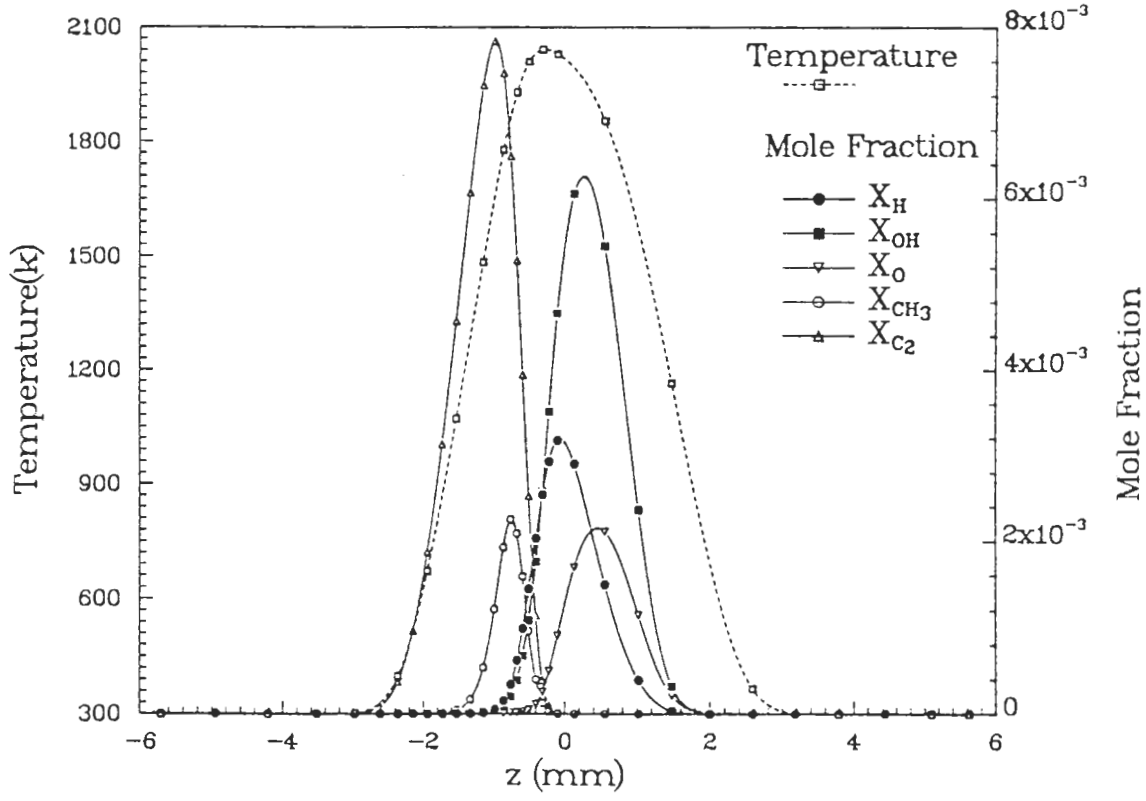

Downloaded from http://asmedigitalcollection.asme.org/GT/proceedings-pdf/GT1996/78743/V003T06A053/2407413/v003t06a053-96-gt-545.pdf by guest

Fig.8a: Predicted profiles of temperature and CH concentration without water.

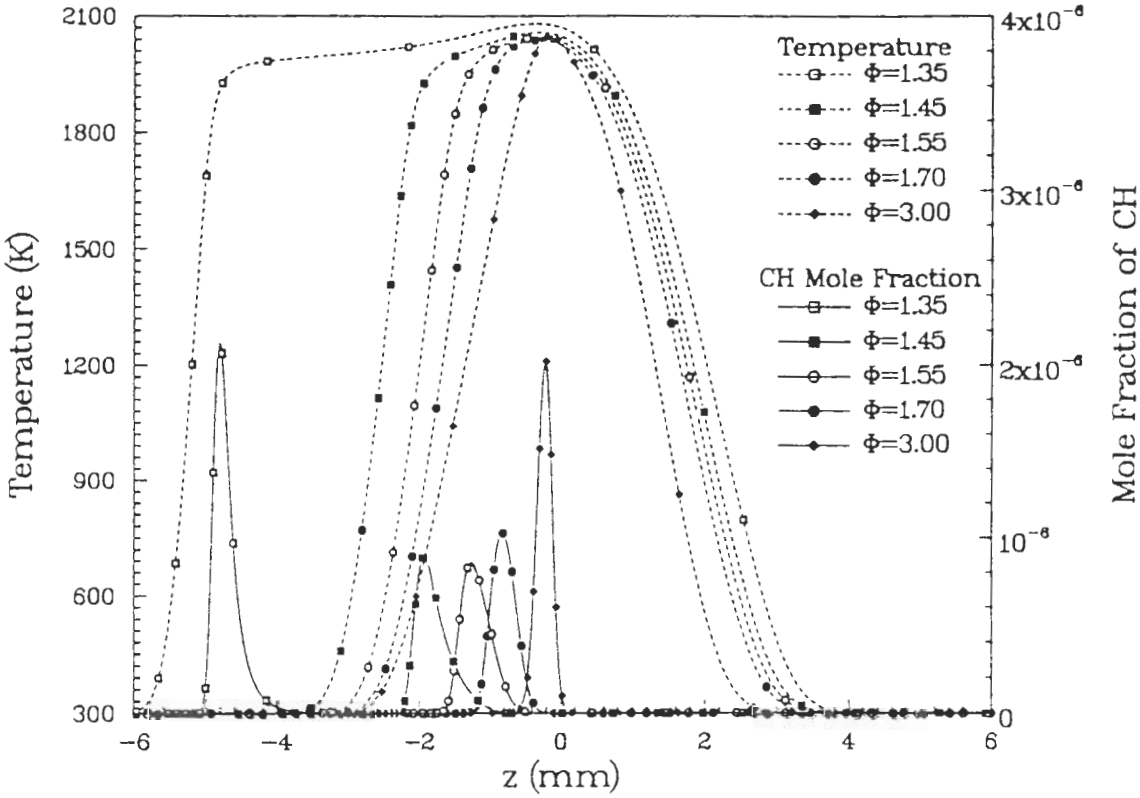

Fig.8b: Predicted profiles of temperature and CH concentration with 10% water added in air stream.

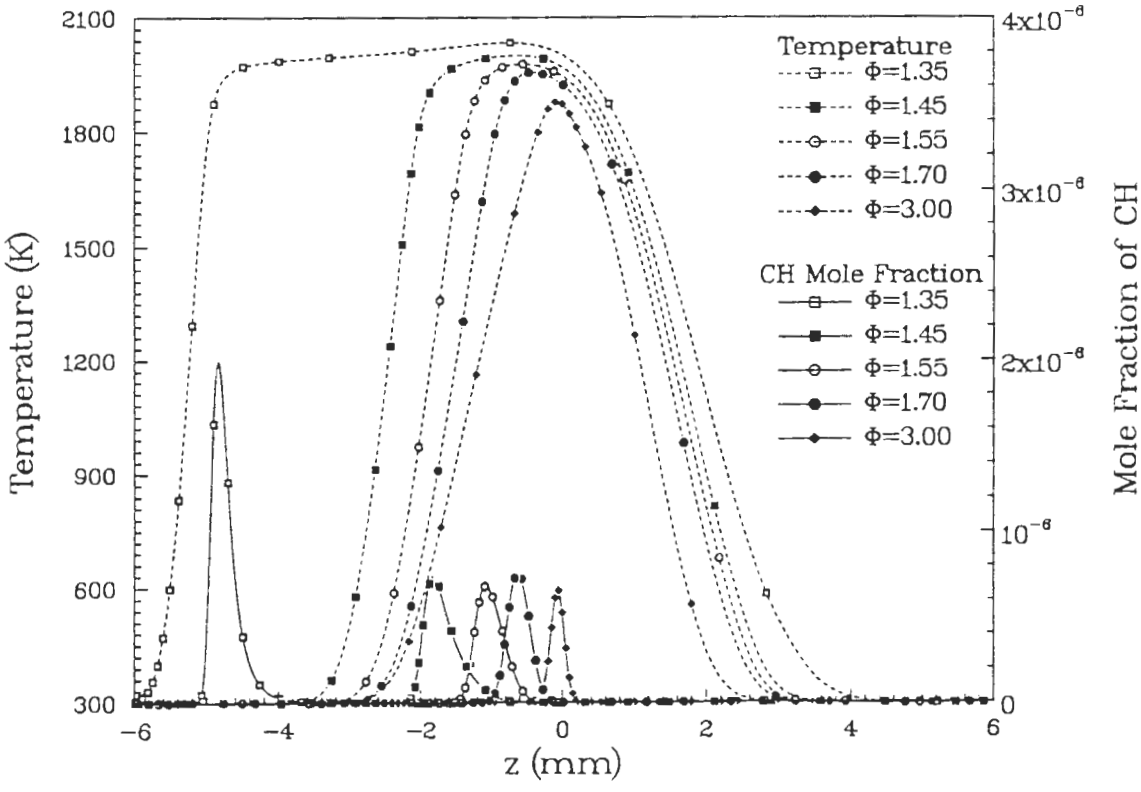

Downloaded from http://asmedigitalcollection.asme.org/GT/proceedings-pdf/GT1996/78743/V003T06A053/2407413/v003t06a053-96-gt-545.pdf by g

Fig.9a: Computed profiles of temperature and N concentration without water.

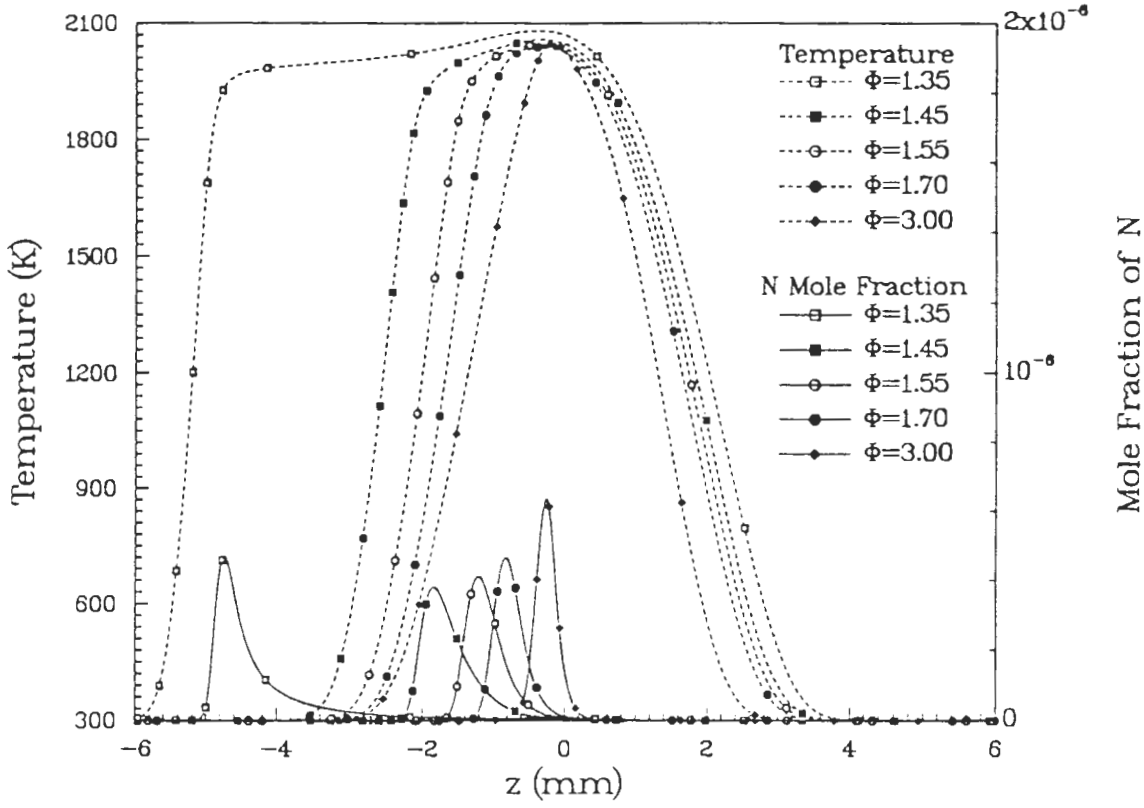

Fig.9b: Computed profiles of temperature and N concentration with 10% water added in air stream.

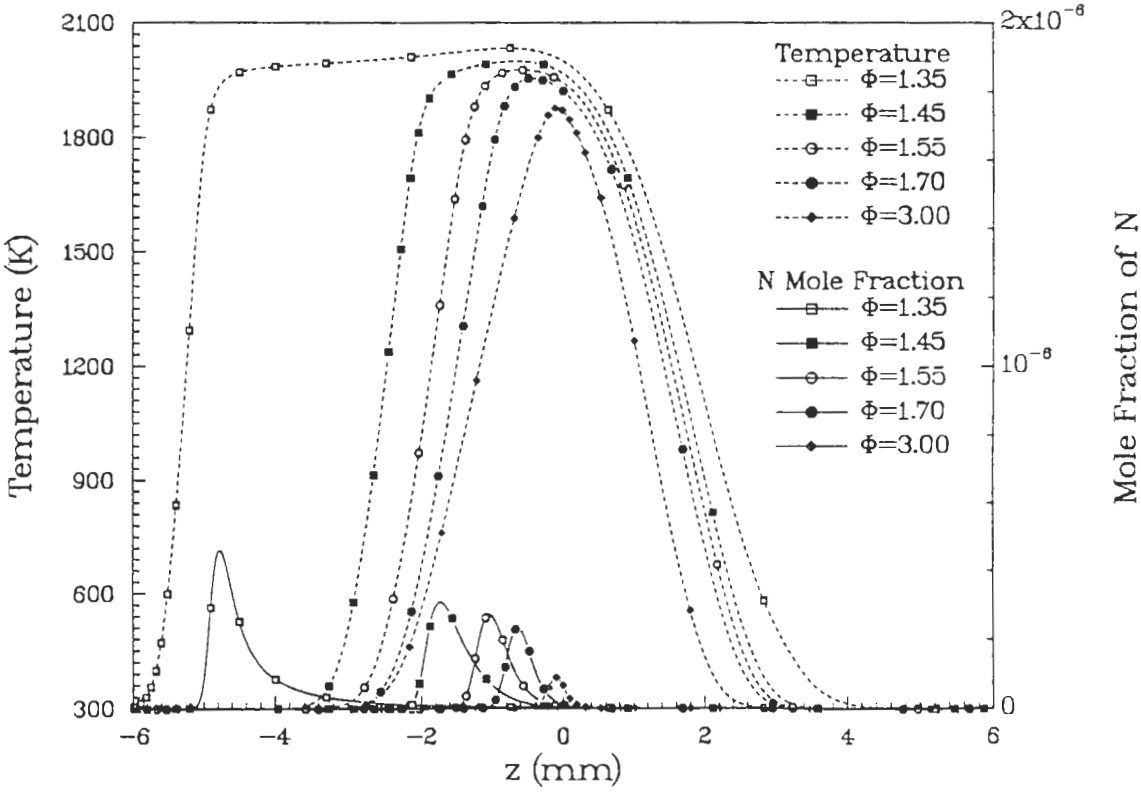

Downloaded from http://asmedigitalcollection.asme.org/GT/proceedings-pdf/GT1996/78743/V003T06A053/2407413/v003t06a053-96-gt-545.pdf by gues

Fig.10a: Computed profiles of temperature and HCN concentration without water.

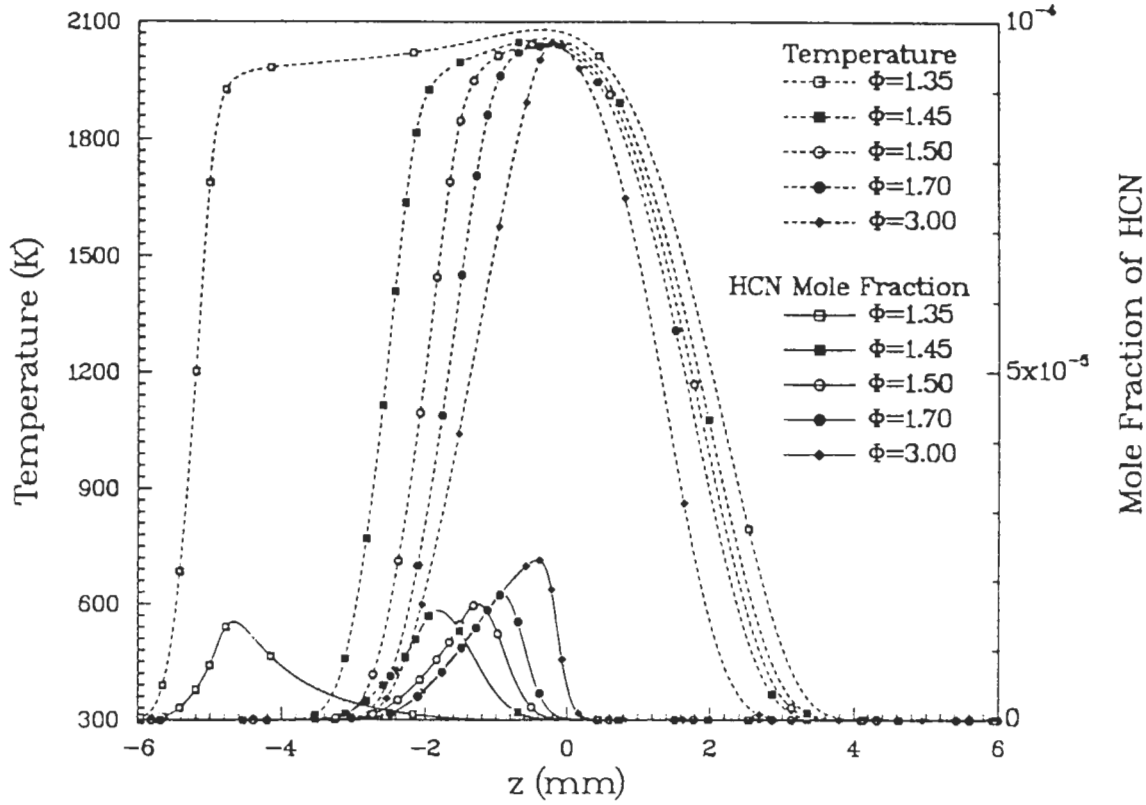

Fig.10b: Computed profiles of temperature and HCN concentration with 10% water added in air stream.

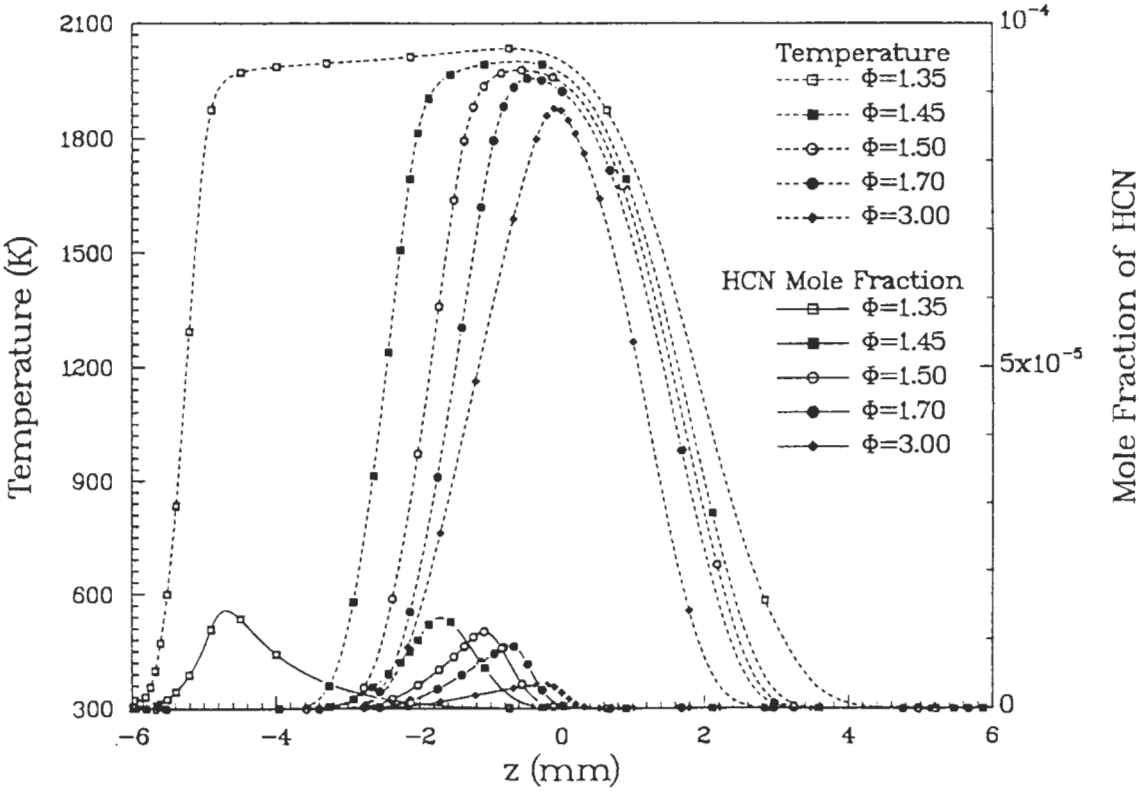

Downloaded from http://asmedigitalcollection.asme.org/GT/proceedings-pdf/GT1996/78743/V003T06A053/2407413/v003t06a053-96-gt-545.pdf by guest

Fig.11: Contributions to NO emission index from various reactions.

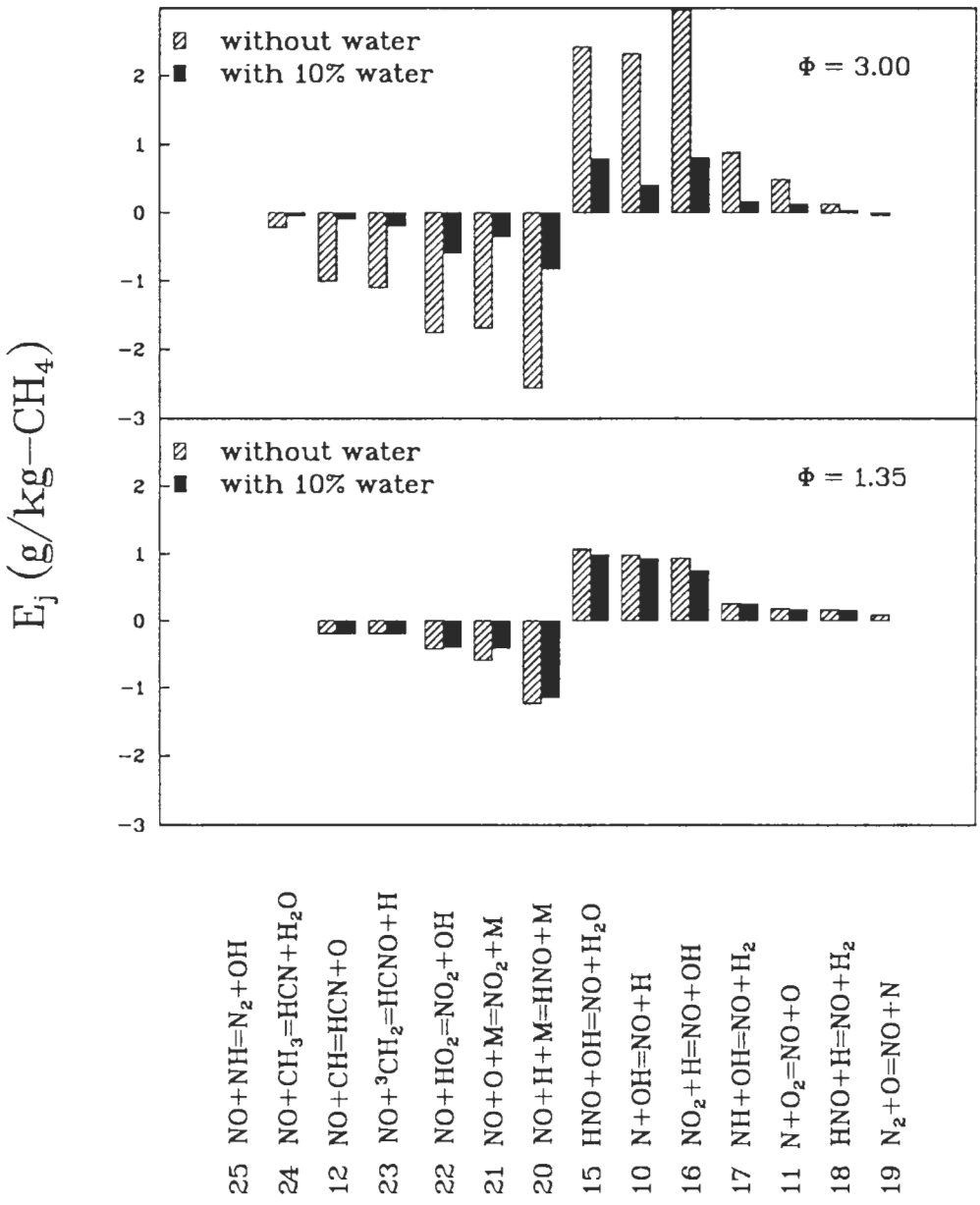

Downloaded from http://asmedigitalcollection.asme.org/GT/proceedings-pdf/GT1996/78743/V003T06A053/2407413/v003t06a053-96-gt-545.pdf by guest

Fig.12a: Computed profiles of temperature and NO concentration without water.

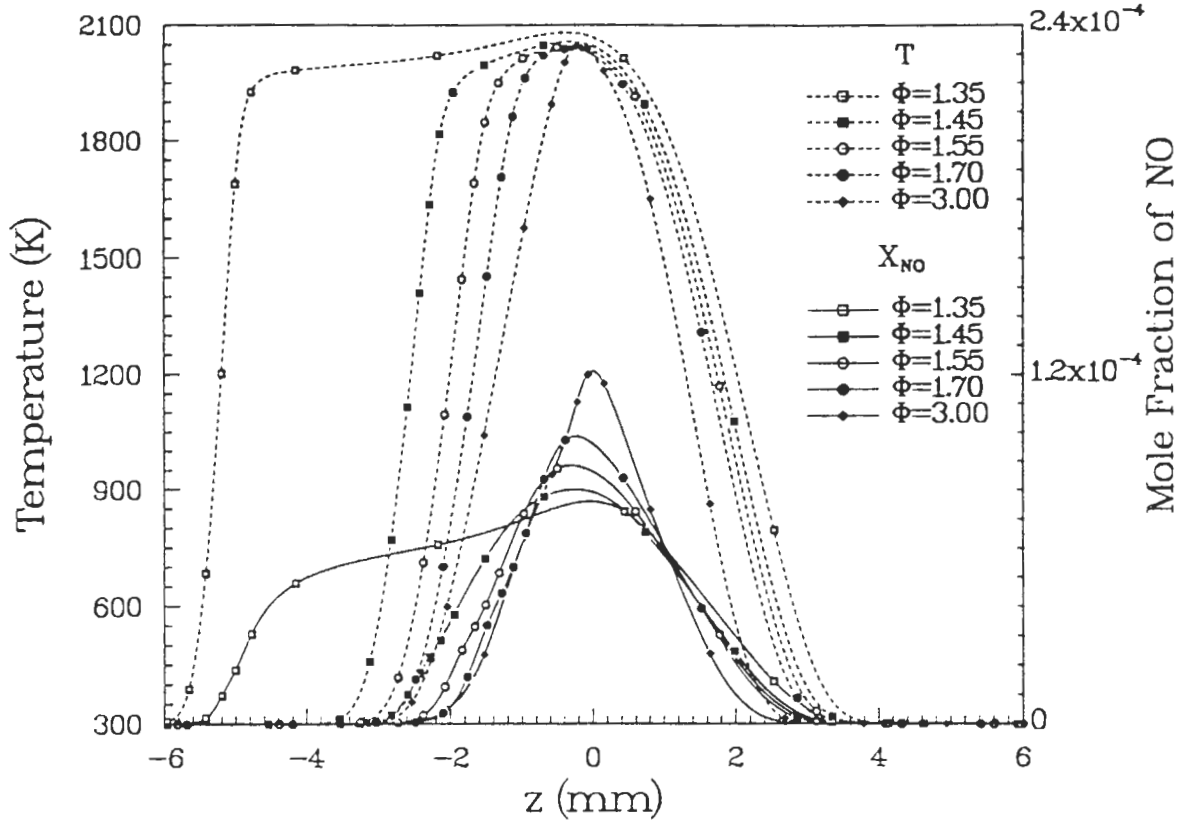

Fig.12b: Computed profiles of temperature and NO concentration with 10% water added in air stream.

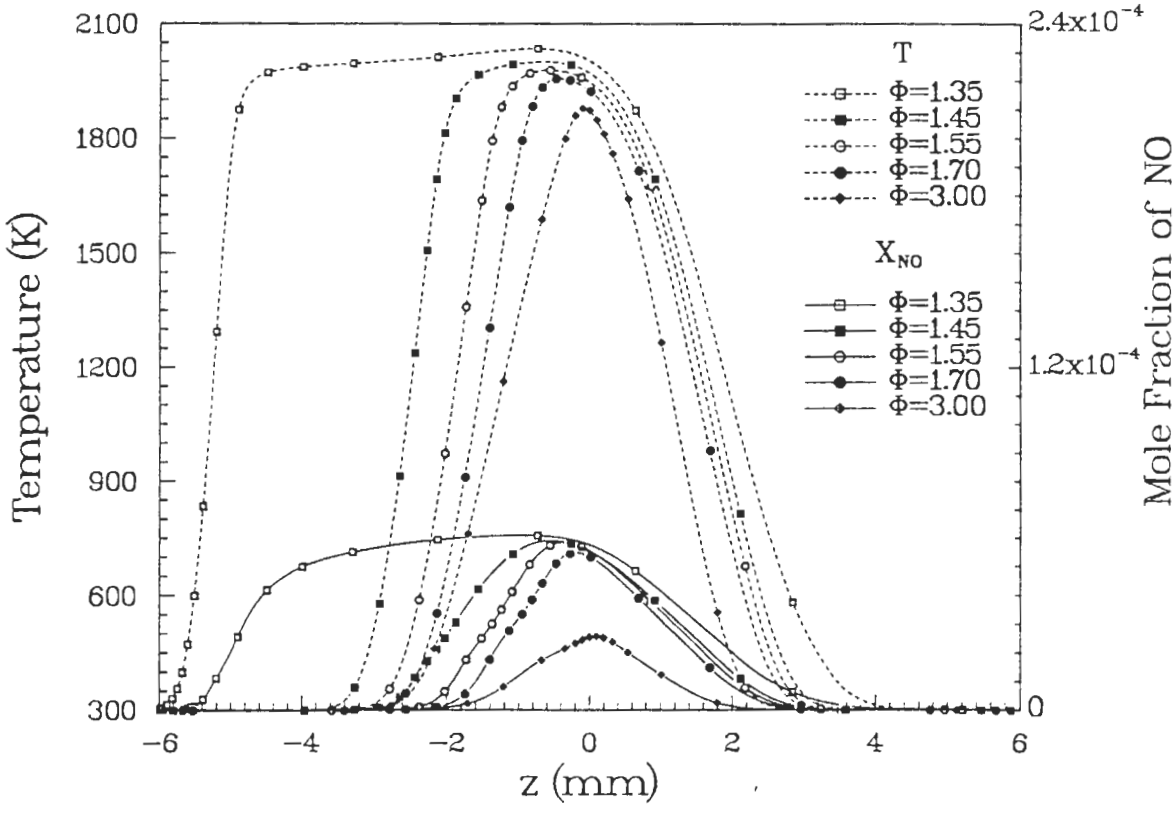

Downloaded from http://asmedigitalcollection.asme.org/GT/proceedings-pdf/GT1996/78743/V003T06A053/2407413/v003t06a053-96-gt-545.pdf by guest

Fig.13: Predicted NO emission index as a function of equivalence ratio and mass percentage of water added to the air stream.

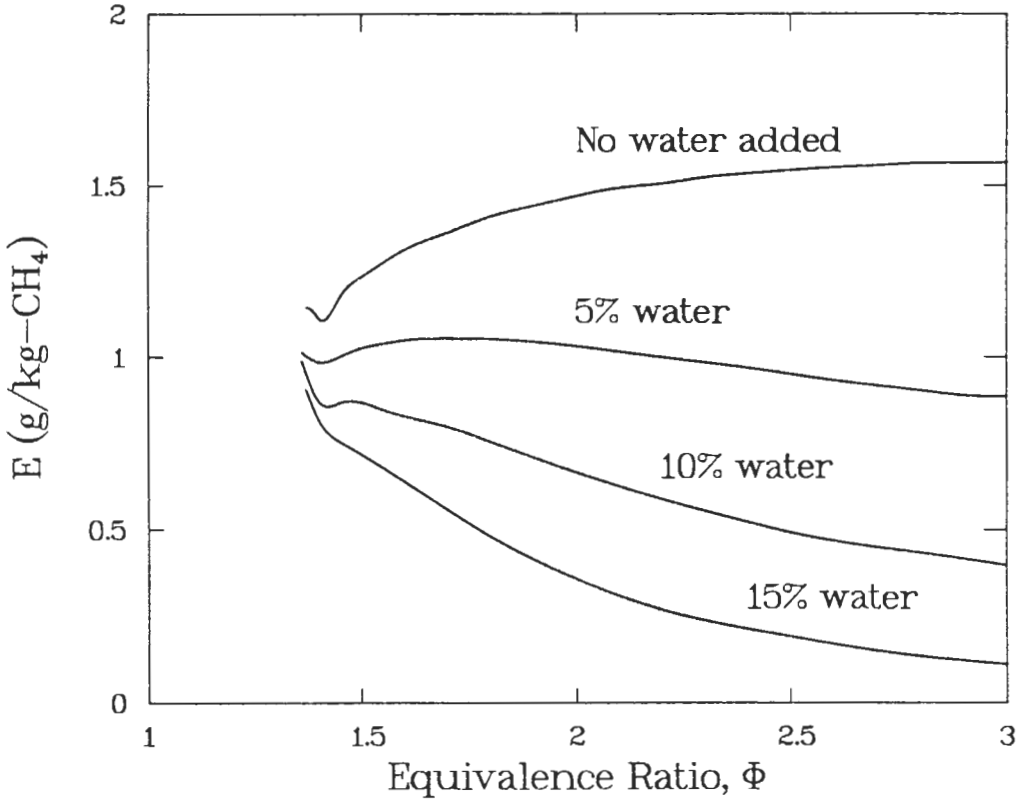

Downloaded from http://asmedigitalcollection.asme.org/GT/proceedings-pdf/GT1996/78743/V003T06A053/2407413/v003t06a053-96-gt-545.pdf by guest